Nonvolatile memory properties of Pt nanoparticle-embedded TiO$_2$ nanocomposite multilayers via electrostatic layer-by-layer assembly

Chanwoo Lee[1], Inpyo Kim[1], Hyunjung Shin[1], Sanghyo Kim[2] and Jinhan Cho[1]

[1] School of Advanced Materials Engineering, Kookmin University, Jeongneung-dong, Seongbuk-gu, Seoul 136-702, Korea
[2] College of BioNano Technology, Kyungwon University, San 65, Bokjeong-dong, Sujeong-gu, Kwonggi-do 461-701, Korea

E-mail: jinhan@kookmin.ac.kr

Abstract
It is demonstrated that notable resistive switching memory properties depending on voltage polarity (i.e. bipolar switching properties) can be obtained from the layer-by-layer (LbL) assembled multilayers based on transition metal oxides and metal nanoparticles. Cationic poly(allylamine hydrochloride) and anionic titania precursor layers were deposited alternately onto Pt-coated Si substrates using an electrostatic LbL assembly process. Anionic Pt nanoparticles (Pt$_{NP}$) with about 5.8 nm diameter size were also inserted within the multilayers using the same interactions mentioned above. These multilayers were converted to Pt$_{NP}$-embedded TiO$_2$ films by thermal annealing and the films were then coated with a top electrode. When external bias was applied to the devices, bipolar switching properties were observed at low operating voltages showing the high ON/OFF ratio ($>10^4$) and the stable device performance. These phenomena were caused by the presence of Pt$_{NP}$ inserted within TMO films.

S Online supplementary data available from stacks.iop.org/Nano/21/185704/mmedia

(Some figures in this article are in colour only in the electronic version)

1. Introduction

Resistive switching nonvolatile memory (RSM) devices with capacitor type in the metal–insulator–metal structure have attracted considerable interest due to the widespread use of mobile electronics such as MP3 players, digital cameras and mobile phones [1–16]. In particular, it has been reported that RSM devices based on transition metal oxides (TMOs) have excellent memory performance, such as large ON/OFF ratio $>10^3$, fast switching speed and low operating voltage in spite of the simple device structure and chemical composition. Generally, binary TMOs [1–4, 8, 9] such as TiO$_2$ or NiO are used as resistance switching materials

exhibiting a significant change in resistance between the high resistance state and low resistance state under applied voltage sweep. Recently, many efforts have been made to modify or improve the electrical properties of RSM devices through the insertion of electrically functional components within TMO matrices [12–15]. However, the vacuum deposition process used for preparation of TMO has great difficulty in building large-area devices at low cost with a simplified manufacturing process and easily inserting a variety of electrically active components (i.e. metal or inorganic nanoparticles) within TMO matrices, although TMO materials have excellent thermal stability and operating durability in air environment. As an alternative, soluble polymers may be considered to be

promising candidates for the active layers in future nonvolatile memory devices because they can be deposited by facile solution processes such as spin-coating [17–20].

One of the proposed models for resistive switching is that electronic charges are injected by Fowler–Nordheim tunneling at high electric fields and subsequently trapped at sites such as defects (i.e. grain boundaries, residual carbons or oxygen deficiency states) in the insulators. Therefore, the memory effect with the high and low current states can occur from charge storage (high resistance) and release (low resistance) within the charge trap sites, and furthermore a degree of charge storage and release can have a significant effect on current ON/OFF ratio and device stability. This model suggested to us intriguing new possibilities for designing RSM devices with improved memory properties. The key to these design schemes is based on an electrostatic layer-by-layer (LbL) assembly process [21–33], which is quite useful for preparing nanocomposite multilayer films with tailored nanostructures as well as the insertion of various functional components. This approach is achieved by tuning the electrostatic interactions between oppositely charged components. More specifically, anionic titanium(IV) bis(ammonium lactato)dihydroxide (TALH) as a titania precursor can be electrostatically assembled with cationic poly(allylamine hydrochloride) (PAH), allowing the formation of multilayers [30–32], and furthermore negatively charged Pt nanoparticles (Pt_{NPs}) can be easily inserted within TALH/PAH multilayers using the same LbL solution process. The subsequent thermal treatment of the resulting multilayers can yield the TiO_2 nanocomposite films with Pt_{NP} layers at defined placement via thermal decomposition of organic components.

Herein, we demonstrate that RSM devices based on Pt_{NP}-embedded TiO_2NC has a bipolar switching property depending on the polarity of the applied voltage with low operating voltages, large ON/OFF ratios ($\sim 10^4$), long retention times and excellent environmental stability. On the other hand, TiO_2NC devices without Pt_{NPs} exhibited unstable bipolar switching behavior with a relatively low ON/OFF ratio (<10). These evident differences in electrical performance between TiO_2NC- and Pt_{NP}-embedded TiO_2NC were caused by the presence of metal nanoparticles operating as deep charge trap sites, which were confirmed from the changes in real-space imaging of the charge trap and release state as a function of time. This work is significant because it provides a tool for easily constructing RSM devices based on solution-processible inorganic multilayers with flexible switching properties. We also believe that our approach can be effectively used for many potential electronic applications requiring high performance, long durability, large-area scale and low fabrication cost in air environment.

2. Experimental part

2.1. Preparation of TiO_2 nanocomposite films from Pt_{NP}-embedded $(PAH/TALH)_n$ multilayers

The concentration of PAH ($M_w = 70\,000$, Aldrich) and TALH (Aldrich) solutions used for all the experiments was 1 and 50 mg ml^{-1} [32]. Pt-coated Si substrates had an anionic surface by irradiating UV light. These substrates were first dipped for 10 min in the cationic PAH solution (containing 0.5 M NaCl), washed twice by dipping in water for 1 min and air-dried with a gentle stream of nitrogen. Anionic TALH was subsequently deposited onto the PAH-coated substrates by using the same adsorption, washing and drying procedures as described above. In addition, the anionic Pt_{NP} stabilized by citrate ions was inserted within $(PAH/TALH)_n$ multilayers. The resultant multilayer films were thermally annealed at 450 °C for 2 h under nitrogen and additionally annealed at the same temperature for 2 h under oxygen conditions.

2.2. QCM measurements

A QCM device (QCM200, SRS) was used to investigate the mass of material deposited after each adsorption step. The resonance frequency of the QCM electrodes was approx. 5 MHz. The adsorbed mass of PAH and TALH, Δm, can be calculated from the change in QCM frequency, ΔF, according to the Sauerbrey equation: ΔF (Hz) $= -56.6\Delta m_A$, where Δm_A is the mass change per quartz crystal unit area in μg cm^{-2}.

2.3. Surface morphology

The surface morphology and roughness of thermally annealed TiO_2NC onto Si substrates were measured with an atomic force microscope (AFM) in tapping mode (SPA400, SEIKO).

2.4. Crystal structure

The crystal structure of LbL TiO_2 NC was investigated using x-ray diffraction (XRD) at room temperature. Data collection was performed in the 2θ range from 15° to 60° using Cu Kα radiation ($\lambda = 1.54$ Å, Model: Bruker D8 Discover, Germany). Cross-sectional TEM (Model: JEOL 300kV) was also used to investigate the TiO_2 crystal structure and the internal structure of nanocomposite multilayers.

2.5. Fabrication of resistive switching memory devices

All the samples were prepared on Si substrates (2 cm × 2 cm) with an SiO_2 layer of about 100 nm thickness. A Ti layer of 20 nm thickness was then deposited on the substrates and a bottom electrode (Pt) was subsequently deposited using a DC-magnetron sputtering system. The $(PAH/TALH)_n$ multilayer films were then formed on the Pt-coated Si substrates. The resultant multilayer films were thermally annealed at 450 °C for 2 h under nitrogen and additionally annealed at the same temperature for 4.5 h under oxygen conditions. After thermal conversion, top electrodes (Ag) with 100 μm diameter were deposited onto the nanocomposite films. To investigate the resistive switching behavior of LbL multilayered devices, the current–voltage (I–V) curves were measured by a semiconductor parametric analyzer (SPA, Agilent 4155B) in air environment. The pulsed voltage duration dependence of high and low current states was investigated using a semiconductor parametric analyzer (HP 4155A) and pulse generator (Agilent 81104A).
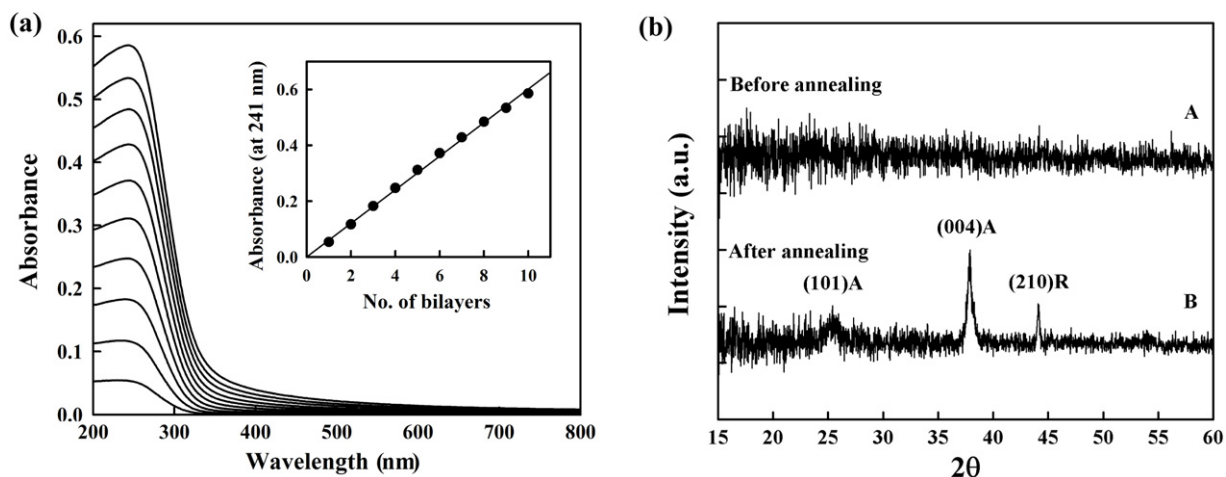
Figure 1. (a) UV–vis spectra of (PAH/TALH)$_n$ multilayers measured with increasing bilayer number (n). The inset of (a) shows the absorbance of TALH measured at 241 nm as a function of bilayer number. (b) XRD patterns of (PAH/TALH)$_n$ multilayers (A) before and (B) after thermal annealing at 450 °C.

3. Results and discussion

For the preparation of Pt$_{NP}$-embedded nanocomposite multilayers, a cationic PAH, anionic titanium(IV) bis(ammonium lactato)dihydroxide (TALH) and citrate ion-stabilized Pt$_{NP}$ of approximately 6 nm size were used (see supporting information, figure S1, available at stacks.iop.org/Nano/21/185704/mmedia). Anionic Pt nanoparticles (Pt$_{NP}$) were synthesized as follows [34]: 250 ml of 1.79 mM H$_2$Cl$_6$Pt · 6H$_2$O was maintained at room temperature with vigorous stirring. Rapid addition of 20 ml of 68 mM sodium citrate to the vortex of the solution and successive addition (1 ml) of 70 mM NaBH$_4$ resulted in a color change from dark yellow to dark brown. The diameter of synthesized Pt$_{NP}$ was about 5.8 ± 1 nm (100 particles sampled) as confirmed by transmission electron microscopy (TEM) images.

First, the LbL assembly of PAH and TALH was performed on quartz substrates, and the growth of the multilayers was monitored by UV–vis spectroscopy. The uniform increase in the intensity of the absorbance peak at 241 nm (due to TALH) suggests that a regular amount of TALH was adsorbed per bilayer, demonstrating PAH/TALH multilayer growth (figure 1(a)). The inset in figure 1(a) shows that the absorbance at 241 nm increased linearly with increasing bilayer number of PAH/TALH. Based on this electrostatic LbL assembly, anionic Pt$_{NP}$ were inserted within the PAH/TALH multilayers. In particular, electrostatic repulsion between the same charged Pt$_{NPs}$ could induce the adsorption of dispersed Pt$_{NPs}$ onto the positively charged PAH-coated substrate, allowing these nanoparticles to be used as isolated charge trap elements. These multilayers could be converted easily to Pt$_{NP}$–TiO$_2$ multilayer films by thermal degradation of the organic components when annealed at 450 °C. The fully thermal decomposition of organic compounds in the films was confirmed from thermogravimetric analysis (see supporting information, figure S2, available at stacks.iop.org/Nano/21/185704/mmedia). In this case, the total film thickness of the multilayers was reduced to approximately 53% of the initial film thickness and the formed TiO$_2$ nanocomposites showed a strong growth of a typical anatase (004) plane peak and relatively weak rutile crystal (210) plane peak, as confirmed by x-ray diffraction (XRD) patterns (figure 1(b)) [32].

Based on these results, three types of TiO$_2$ nanocomposite (TiO$_2$NC) devices were prepared with increasing amounts of Pt$_{NP}$ inserted within the nanocomposite, as shown in figure 2. The total thicknesses of these multilayers were approximately 40 nm for (TiO$_2$NC)$_{30}$ and [(TiO$_2$NC)$_{12}$(Pt$_{NP}$)$_1$]$_2$/(TiO$_2$NC)$_4$, and 50 nm for [(TiO$_2$NC)$_3$/(Pt$_{NP}$)$_1$]$_7$/(TiO$_2$NC)$_2$ films. In this case, the total Pt$_{NP}$ number densities of [(TiO$_2$NC)$_{12}$(Pt$_{NP}$)$_1$]$_2$/(TiO$_2$NC)$_4$ and [(TiO$_2$NC)$_3$/(Pt$_{NP}$)$_1$]$_7$/(TiO$_2$NC)$_2$ films were measured to be 3.7×10^{12} cm^{-2} and 1.3×10^{13} cm^{-2}, respectively. (The density, volume and mass per one Pt$_{NP}$ were 21.5 g cm^{-3}, 1.0×10^{-19} cm^3 and 2.2×10^{-18} g, respectively. In addition, the frequency and mass change per Pt$_{NP}$ layer were about 230 Hz and 4.1 μg cm^{-2}.)

For measurements of typical bipolar switching, a top Ag electrode was deposited onto the resulting multilayers and a voltage sweep from −2 to +2 V and back to −2 V was applied after an electroforming process at approximately 2.5 V with limited current compliance up to 100 mA. When the voltage polarity applied to the nanocomposite devices was reversed, the high current state (scan range > ±2 V) that had formed after electroforming was converted suddenly to a low current state at +1.5 V (i.e. RESET voltage) (figure 3). When the applied voltage was increased from +2 to −2 V (e.g. regions (3) and (4)), the device with the low current state ('OFF' state) showed an abrupt increase in current of approximately −1.9 V (i.e. SET voltage). It should be noted that the [(TiO$_2$NC)$_{12}$/(Pt$_{NP}$)$_1$]$_2$/(TiO$_2$NC)$_4$ devices exhibited significant bipolar switching behavior with high ON/OFF ratio >10^4 compared to the (TiO$_2$NC)$_{30}$ devices, which showed poor and unstable nonvolatile characteristics with relatively low ON/OFF current ratio <10. This bipolar switching phenomenon was also observed in the voltage
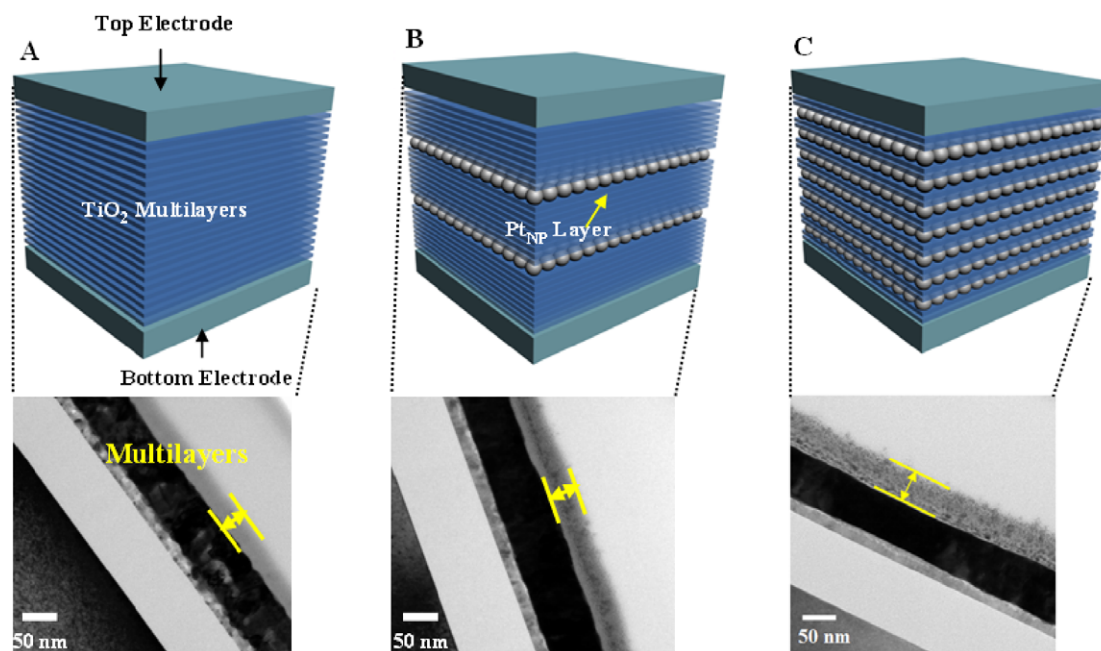
Figure 2. Schematic and TEM images for Pt$_{NP}$-embedded TiO$_2$NC multilayers with three different structures. (A) (TiO$_2$NC)$_{30}$, (B) [(TiO$_2$NC)$_{12}$/(Pt$_{NP}$)$_1$]$_2$/(TiO$_2$NC)$_4$ and (C) [(TiO$_2$NC)$_3$/(Pt$_{NP}$)$_1$]$_7$/(TiO$_2$NC)$_2$.

sweep from $+2$ to -2 V and back to $+2$ V. In view of the practical device applications, the electrical stability of the [(TiO$_2$NC)$_{12}$/(Pt$_{NP}$)$_1$]$_2$/(TiO$_2$NC)$_4$ device was also comparable to that of the conventional vacuum-deposited devices. The ON and OFF states of the device at two different reading voltages of ± 0.1 V were kept continuously stable during the entire test period of 10^4 s under atmospheric conditions (figure 3(b)). This device was operated at an applied voltage pulse ($+4$ V for SET and -1 V for RESET) with a 100 ns pulse width (figure 3(c)). The slight increase in the ON/OFF current ratio was caused by the increase pulsed voltage duration from 100 ns to 1 ms. However, the stable bipolar switching behavior of the Pt$_{NP}$-inserted devices was strongly dependent on the amount of Pt$_{NP}$ inserted within the nanocomposite multilayers. The further insertion of Pt$_{NP}$ layers (more than three Pt$_{NP}$ layers) yielded electrically shorted devices. In other words, the [(TiO$_2$NC)$_3$/(Pt$_{NP}$)$_1$]$_7$/(TiO$_2$NC)$_2$ multilayer structure with a particle number density of 1.3×10^{13} cm^{-2} showed metallic properties without resistive switching. (The particle number density was calculated from the particle size, density and adsorbed mass per unit area measured from a quartz crystal microbalance.)

According to the Simmons–Verderber model [34], the memory effect with the high and low current states was due to charge storage (high resistance) and release (low resistance) within the charge trap sites. In this system, the Pt$_{NP}$ within the TiO$_2$NC matrix can be used as charge trap elements, which can affect the switching mechanism considerably. First, after initial electroforming, the negative voltage sweep of devices from -2 to 0 V releases the electrons from Pt$_{NP}$s (e.g. (1)). When electrons are partially injected in Pt$_{NP}$ (e.g. (2)) and trapped in Pt$_{NP}$ by reversing the voltage polarity (e.g. (2) $\rightarrow$ (3)), the conductive filament paths for electrons in the TiO$_2$NC

matrix are broken down, resulting in a decrease in conductivity, corresponding to the RESET process. This state is maintained up to about -1.9 V (e.g. region (4)). However, an increase of external electric field for releasing the trapped electrons within Pt$_{NP}$s (e.g. region (4)) is thought to sharply increase the conductivity at SET voltage (i.e. $V_{SET} \approx -1.9$ V) enhancing tunneling probability (i.e. SET process). These processes are repeated reversibly. However, the proposed mechanism has a difficulty in understanding electron transport in the TiO$_2$ matrix. Recently, a memristive mechanism of TiO$_2$ has been reported extensively from mainly Hewlett-Packard labs [8, 9]. That is, the oxygen vacancies repelled or attracted from the top electrode according to the electric field can be drifted, and as a result may have a significant effect on the electronic barrier for electron transport at the interface between electrode and TiO$_2$. In this view, the bipolar switching behavior of TiO$_2$NC without Pt$_{NP}$s can be understood by a memristor model. On the other hand, in the case of Pt$_{NP}$-embedded TiO$_2$NC showing relatively high ON/OFF current ratio, their switching behavior can be influenced by the electron trap within Pt$_{NP}$s as well as the electron transport in the TiO$_2$ matrix, as mentioned above.

Considering that a variety of defects, such as oxygen vacancies, dislocations and grain boundaries, can be used as charge trap sites, the Pt$_{NP}$ in the TiO$_2$NC matrix can operate as a relatively deep charge trap site. In order to test this possibility, Kelvin force microscopy (KFM) was used to examine the changes in real-space imaging of the charge trap and release state as a function of time as previously reported by our group [35]. The charges stored within each Pt$_{NP}$s could be detected from the change in surface potential when the tip (i.e. Au-coated tip with 20 nm diameter) of the KFM scans the surface of the TiO$_2$ layer covering the Pt$_{NP}$s. First, a $1.5 \times 1.5 \ \mu$m^2 area of TiO$_2$ and Pt$_{NP}$-inserted TiO$_2$ films was
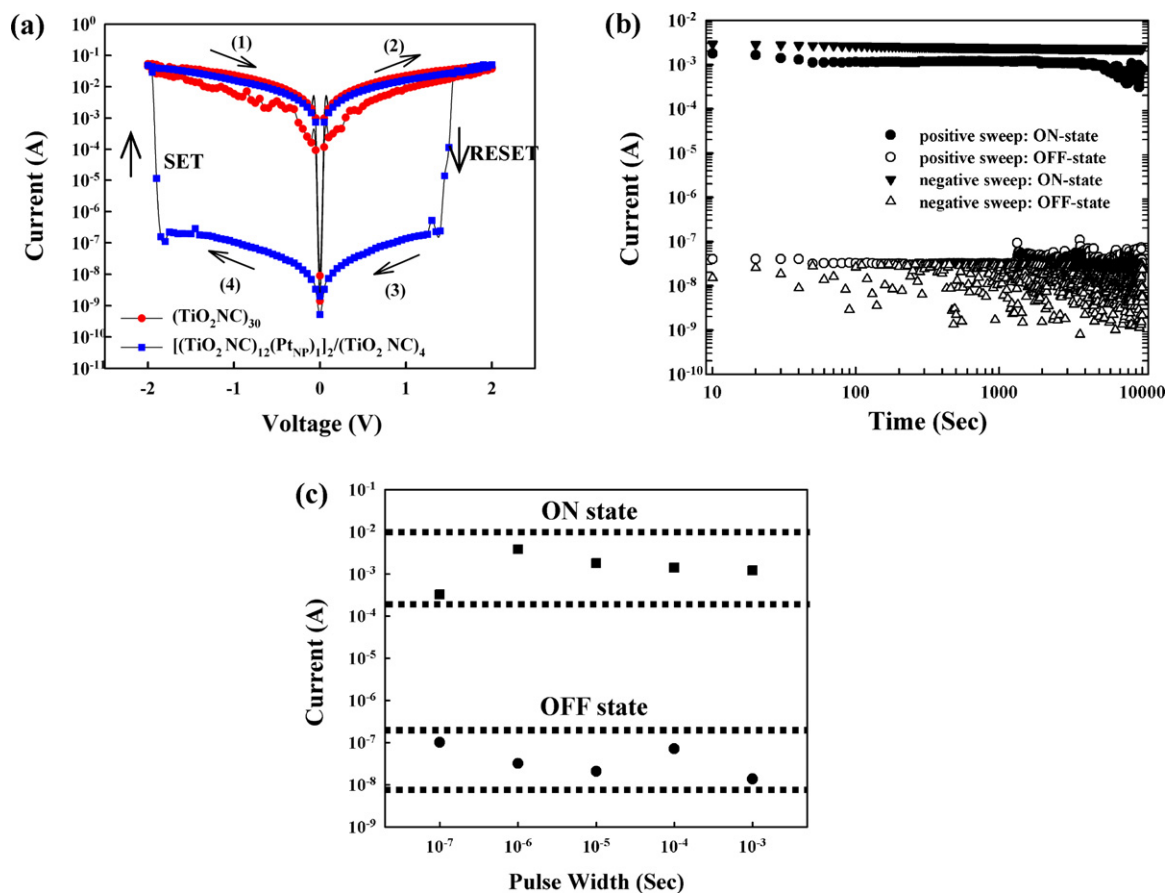
Figure 3. (a) I–V curves of TiO$_2$NC multilayers with different Pt$_{NP}$ layer number and without Pt$_{NP}$. After initial electroforming process (current compliance of 100 mA), the applied voltage was scanned from −2 to 2 V and then reversed from 2 to −2 V. (b) Retention time test of [(TiO$_2$NC)$_{12}$/(Pt$_{NP}$)$_2$]$_3$/(TiO$_2$NC)$_4$ multilayer device. The high and low conductive states were induced using reading voltages of +0.1 V (positive sweep) and −0.1 V (negative voltage sweep). (c) The ON current values at 4 V and OFF current values at −1 V for different pulse widths (100 ns, 1 μs, 10 μs and 100 μs) using reading voltages of ±0.1 V.

scanned at −8 V and −4 V for the charge trap, respectively. After that, the charge release operation was successively performed by scanning a 500 × 500 nm^2 area with a +8 V (for the TiO$_2$ device) and +4 V bias (for the Pt$_{NP}$-inserted TiO$_2$ device) applied to the bottom contact. As shown in figure 4, the yellow region indicates a charge trap state and the dark region corresponds to the charge release state. Although the TiO$_2$ and Pt$_{NP}$–TiO$_2$ films had charge trap sites, as shown by the color contrast (i.e. potential difference between the charge trap and charge release state), there was a clear difference in charge trap depth between the diffuse (for TiO$_2$NC) and charge trap images (for Pt$_{NP}$-inserted TiO$_2$NC), according to the presence of Pt$_{NP}$. If −4 V and +4 V were applied to the TiO$_2$ device for charge trap and release, respectively, the diffuse images of KFM would have considerable difficulty in distinguishing between the charge trap and release state due to their shallow trap sites. In addition, the charge stored state of the TiO$_2$ film device decayed rapidly (70% decrease in color contrast after 30 min) compared to that of the Pt$_{NP}$-inserted TiO$_2$ film device (50% decrease in color contrast after 90 min). On the other hand, we did not observe any notable change in topographic images with increasing time. This suggests that the Pt$_{NP}$ in TiO$_2$ films can operate effectively as deep charge trap elements. It

should be noted here that the retention test shown in figure 3(b) cannot be directly made a comparison with charge trap decay in KFM analysis because the surface environment of the TiO$_2$ nanocomposite is totally different. More specifically, the oxide surface for the retention test was sandwiched between two metal electrodes, which can block the formation of a contaminant layer (i.e. surface water layer or surface hydroxyl group) onto the oxide surface. On the other hand, the oxide surface for KFM analysis was exposed to the air. Sugimura *et al* reported that the increase of surface hydroxyl groups on the oxide layer decreases the potential contrast in KFM images [36]. Therefore, charge trap decay analysis of Pt$_{NP}$-embedded TIO$_2$NC cannot be quantitatively compared with the retention test of Pt$_{NP}$-embedded TiO$_2$NC sandwiched between metal electrodes, and the relative comparison in KFM images of the two different devices can be allowed.

Even if it was reported that solid electrolytes sandwiched between an Ag (or Cu) anode and an inert cathode can cause bipolar switching behavior via an electrochemical redox reaction based on the high mobility of Ag ions [37], and furthermore metal ion diffusion from the top electrode can form localized metal atom chains that bridge the electrode materials under an electric field [38–40], our device also
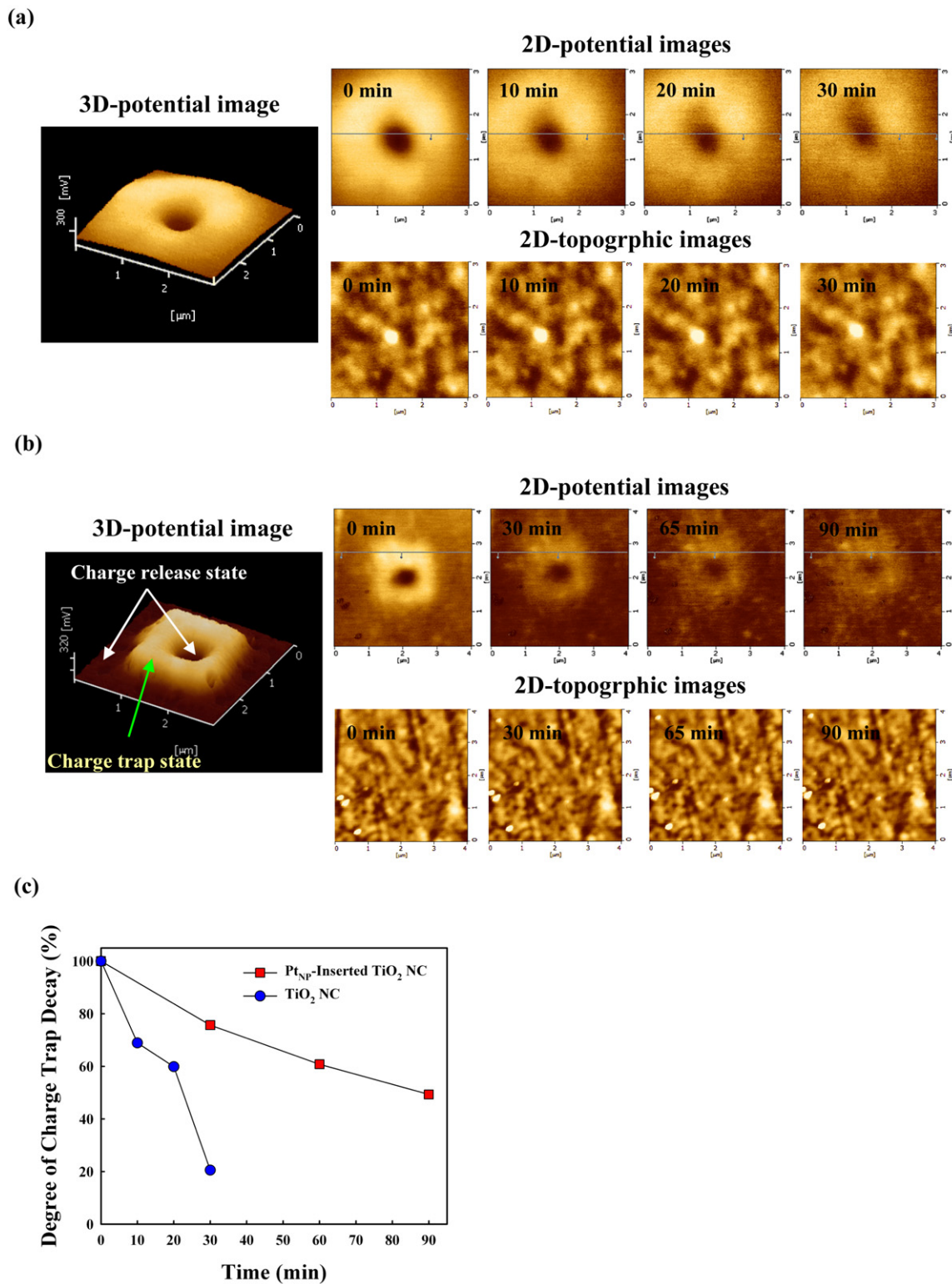
(a)

(b)

(c)

Figure 4. KFM images of (a) TiO$_2$NC-and (b) Pt$_{NP}$-inserted TiO$_2$NC devices as a function of time. (c) Degree of charge trap decay in TiO$_2$NC-and Pt$_{NP}$-inserted TiO$_2$NC devices. In this case, the degree of charge trap decay was measured by the color contrast between charge trap and charge release states.

showed bipolar switching behavior from the tungsten top electrode. This phenomenon suggests that the Ag electrode itself has no significant effect on the resistive switching behavior of LbL TiO$_2$NC with Pt$_{NP}$.

4. Conclusions

We demonstrated that RSM devices based on TMO and metal nanoparticles could be easily prepared from the LbL assembly

process and the selective insertion of Pt$_{NP}$ in the center of TMO matrices could significantly improve the ON/OFF ratio and device stability. The notable switching property in our system can be explained by the presence of isolated but homogeneous Pt$_{NP}$ operating as deep charge trap sites. In particular, the changes in real-space imaging of the charge trap and release state as a function of time evidently indicated the difference of charge trap decay between the shallow trap state in TiO$_2$NC- and the deep charge trap states in Pt$_{NP}$-embedded TiO$_2$NC, and as a result support our switching mechanism. We also highlight the fact that our approach allows the production of resistive switching active films with large-area and hybrid structures using a simplified solution process.

Acknowledgments

References

[1] Waser R and Aono M 2007 *Nat. Mater.* **6** 833
[2] Choi D, Lee D, Sim H, Chang M and Hwang H 2006 *Appl. Phys. Lett.* **88** 082904
[3] Rozenberg M J, Inoue I H and Sánchez M J 2004 *Phys. Rev. Lett.* **92** 17802
[4] Sánchez M J, Rozenberg M J and Inoue I H 2006 *Appl. Phys. Lett.* **88** 033510
[5] Weitz R T, Walter A, Engl R, Sezi R and Dehm C 2006 *Nano Lett.* **6** 2810
[6] Schoen D T, Xie C and Cui Y 2007 *J. Am. Chem. Soc.* **129** 4116
[7] Jung Y, Lee S-H, Ko D-K and Agarwal R 2006 *J. Am. Chem. Soc.* **128** 14026
[8] Strukov D B, Snider G S, Stewart D R and Williams R S 2008 *Nature* **453** 80
[9] Yang J J, Pickett M D, Li X, Ohlberg D A A, Stewart D R and Williams R S 2008 *Nat. Nanotechnol.* **3** 429
[10] Barman S, Deng F and McCreery R C 2008 *J. Am. Chem. Soc.* **130** 11073
[11] Kozicki M N, Yun M, Hilt L and Singh A 1999 *Solid State Ionic Devices: Proc. Int. Symp.* (Pennington, NJ: Electrochemical Society) p 298
[12] Chang W-Y, Cheng K-J, Tsai J-M, Chen H-J, Chen F, Tsai M-J and Wu T B 2009 *Appl. Phys. Lett.* **95** 042104
[13] Kim D C *et al* 2006 *Appl. Phys. Lett.* **88** 202102
[14] Liu L F, Kang J F, Xu N, Sun X, Chen C, Sun B, Wang Y, Liu X Y, Zhang X and Han R Q 2008 *Japan. J. Appl. Phys.* **47** 2701
[15] Guan W, Long S, Jia R and Liu M 2007 *Appl. Phys. Lett.* **91** 062111
[16] Lee C, Kim I, Choi W, Shin H and Cho J 2009 *Langmuir* **25** 4274
[17] Ouyang J, Chu C-W, Szmanda C R, Ma L and Yang Y 2004 *Nat. Mater.* **3** 918
[18] Joo W-J, Choi T-L, Lee J, Lee S K, Jung M-S, Kim N and Kim J M 2006 *J. Phys. Chem.* B **110** 23812
[19] Lauters M, McCarthy B, Sarid D and Jabbour G E 2006 *Appl. Phys. Lett.* **89** 013507
[20] Beinhoff M, Bozano L D, Scott J C and Carter K R 2005 *Macromolecules* **38** 4147
[21] Decher G 1997 *Science* **277** 1232
[22] Caruso F, Caruso R A and Möwald H 1998 *Science* **282** 1111
[23] Podsiadlo P *et al* 2007 *Science* **318** 80
[24] Shiratori S S and Rubner M F 2000 *Macromolecules* **33** 4213
[25] Dubas S T, Farhat T R and Schlenoff J B 2001 *J. Am. Chem. Soc.* **123** 5368
[26] Yoo P J, Nam K T, Qi J, Lee S-K, Park J, Belcher A M and Hammond P T 2006 *Nat. Mater.* **5** 234
[27] Lee S W, Kim B-S, Chen S, Yang S-H and Hammond P T 2009 *J. Am. Chem. Soc.* **131** 671
[28] Jiang G, Baba A and Advincula R 2007 *Langmuir* **23** 817
[29] Das B C, Batabyal S K and Pal A J 2007 *Adv. Mater.* **19** 4172
[30] Caruso F, Shi X, Caruso R A and Susha A 2001 *Adv. Mater.* **13** 740
[31] Caruso R A, Susha A and Caruso F 2001 *Chem. Mater.* **13** 400
[32] Lee C, Kim I, Shin H, Kim S and Cho J 2009 *Langmuir* **25** 11276
[33] Park J, Kim I, Shin H, Lee M J, Kim Y S, Bang J, Caruso F and Cho J 2008 *Adv. Mater.* **20** 1843
[34] Simmons J G and Verderber R R 1967 *Proc. R. Soc.* **301** 77
[35] Lee J-S, Cho J, Lee C, Kim I, Park J, Kim Y-M, Shin H, Lee J and Caruso F 2007 *Nat. Nanotechnol.* **2** 790
[36] Sugimura H, Ishida Y, Hayashi K, Takai O and Nakagiri N 2002 *Appl. Phys. Lett.* **80** 1459
[37] Terabe K, Hasegawa T, Nakayama T and Aono M 2005 *Nature* **433** 47
[38] Tsunoda K, Fukuzumi Y, Jameson J R, Wang Z, Griffin P B and Nishi Y 2007 *Appl. Phys. Lett.* **90** 113501
[39] Lee D, Seong D-J, Jo I, Xiang F, Dong R, Oh S and Hwang H 2007 *Appl. Phys. Lett.* **90** 122104
[40] Yang Y C, Pan F, Liu Q, Liu M and Zeng F 2009 *Nano Lett.* **9** 1636